Indentation of a pressurized silicon stomach model - A non-invasive study of gastric wall stiffness and pressurized gastric content stiffness

Liao, Donghua; Mark, Esben Bolvig; Nedergaard, Rasmus Bach; Jensen, Lars Rosgaard; Bertoli, Davide; Frøkjær, Jens Brøndum; Yu, Donghong; Zhao, Jingbo; Brock, Christina; Drewes, Asbjørn Mohr

Published in:
Journal of the mechanical behavior of biomedical materials

DOI (link to publication from Publisher):
10.1016/j.jmbbm.2022.105449

Publication date:
2022

Document Version
Publisher's PDF, also known as Version of record

journal of the mechanical behavior of biomedical materials 135 (2022) 105449

Contents lists available at ScienceDirect

Journal of the Mechanical Behavior of Biomedical Materials

journal homepage: www.elsevier.com/locate/jmbbm

Indentation of a pressurized silicon stomach model – A non-invasive study of gastric wall stiffness and pressurized gastric content stiffness

Donghua Liao [a], Esben Bolvig Mark [a], Rasmus Bach Nedergaard [a], Lars Rosgaard Jensen [b], Davide Bertoli [a], Jens Brøndum Frøkjær [c,d], Donghong Yu [e], Jingbo Zhao [a,f], Christina Brock [a,d,g], Asbjørn Mohr Drewes [a,d,g,*]

[a] Mech-Sense, Department of Gastroenterology and Hepatology, Aalborg University Hospital, Aalborg, Denmark
[b] Department of Materials and Production, Aalborg University, Aalborg, Denmark
[c] Mech-Sense, Department of Radiology, Aalborg University Hospital, Aalborg, Denmark
[d] Department of Clinical Medicine, Aalborg University, Aalborg, Denmark
[e] Department of Chemistry and Bioscience, Aalborg University, Aalborg, Denmark
[f] LBP (Chongqing) Pathological Diagnosis Center, Chongqing, China
[g] Steno Diabetes Center North Denmark, Aalborg, Denmark

ARTICLE INFO

Keywords:
Stomach
Stiffness
Non-invasive
Indentation
Modelling

ABSTRACT

Background and aims: Evaluation of gastric wall stiffness and intragastric pressure is essential for detailed assessments of gastric accommodation. However, non-invasive assessments are needed for large scale clinical studies and none of the existing methods takes abdominal wall effect into the calculation. This study aimed to assess gastric wall stiffness and gastric content stiffness as a proxy for intragastric pressure using novel mechanical modeling and non-invasive indentation tests on a silicon stomach model.

Methods: A silicon stomach model (scaling 1:1 with the human stomach) was indented using a pressure algometer at intragastric pressures from 0 to 0.8 kPa. Wall thicknesses and luminal cross-sectional areas along the stomach were measured with ultrasound images. The gastric wall stiffness was compared between measurements from tensile tests on strips cut from the silicon stomach and estimations from a shell indentation model. The pressurized gastric content stiffness was predicted from a bonded two-layer axisymmetric half-space indentation model.

Results: The gastric wall stiffness estimated from the shell indentation model showed no difference to measurements from the mechanical tests on the cutting strips ($p = 0.14$). The predicted gastric content stiffness was strongly associated with the intragastric pressure ($r > 0.83$, $p < 0.001$).

Conclusions: The mechanical model developed in this study can simultaneously predict the gastric wall stiffness and the pressurized gastric content stiffness. In future studies, the method can be applied to reveal intragastric pressure conditions non-invasively via the pressurized gastric content stiffness during gastric accommodation and emptying such as with magnetic resonance imaging.

1. Introduction

Gastric accommodation is an important mechanism of normal gastric physiology (Kindt and Tack, 2006). Accomodation is described by reduced gastric tone, increased compliance, and increased gastric volume, allowing for a dynamic gastric reservoir for food, enabling the volume to increase without a rise in gastric pressure (Azpiroz and Malagelada, 1987; Distrutti et al., 1999; Gregersen and Christensen, 2000; Kindt and Tack, 2006; Febo-Rodriguez et al., 2021). Gastric tone and compliance are responses to gastric wall stiffness, which can be calculated from the intragastric pressure and the gastric configuration changes during a meal (Azpiroz and Malagelada, 1987; Kindt and Tack, 2006; De Zwart et al., 2007). The barostat/tensostat is the only technology that can simultaneously estimate the intragastric pressure and

* Corresponding author. Department of Clinical Medicine, Aalborg University Hospital, Møllerparkvej, DK-9000, Aalborg, Denmark.
E-mail addresses: dl@rn.dk (D. Liao), e.mark@rn.dk (E.B. Mark), r.nedergaard@rn.dk (R.B. Nedergaard), lrj@mp.aau.dk (L.R. Jensen), d.bertoli@rn.dk (D. Bertoli), jebf@rn.dk (J.B. Frøkjær), yu@bio.aau.dk (D. Yu), jingbozhao@hotmail.com (J. Zhao), christina.brock@rn.dk (C. Brock), amd@dcm.aau.dk (A.M. Drewes).

https://doi.org/10.1016/j.jmbbm.2022.105449
Received 16 June 2022; Received in revised form 23 August 2022; Accepted 1 September 2022
Available online 8 September 2022

the gastric volume (Azpiroz and Malagelada, 1987; Kindt and Tack, 2006; De Zwart et al., 2007). However, the invasive feature of the technology limits its adoption in clinical practice and thus gastric accommodation is not assessed routinely.

Intra-abdominal pressure (IAP) can be measured non-invasively using several indentation technologies, including tensiometer and ultrasound tonometry (Van Ramshorst et al., 2011; Tang et al., 2021; Tayebi et al., 2021). With the indentation test on the abdominal surface, the abdominal wall tension, i.e., the indentation stiffness of the abdominal luminal content, which shows significant correlations to the abdominal pressure (Van Ramshorst et al., 2011; Tang et al., 2021; Tayebi et al., 2021), can be estimated. The higher the intra-abdominal pressure, the stiffer the abdominal luminal content. From a mechanical point of view, the theoretical models behind the abdominal luminal content stiffness calculation are based on the model of an axisymmetric indentation on an elastic half-space with homogeneous material properties. In the indentation model with homogeneous material properties, the whole abdomen, including the abdominal wall and the abdominal luminal content, was assumed to be isotropic and homogeneous, where the effect of the abdominal wall on the abdominal content stiffness estimation were not considered.

Several recent studies have used pressurized shell indentation models to predict relationships between the indentation stiffness and the transmural pressure in spherical and ellipsoidal cells (Vella et al., 2012; Staunton et al., 2016; Sun and Paulose, 2021). The cell wall stiffness can be estimated from indentation responses at the zero-pressure state using the shell indentation models. In contrast, the transmural pressure of the cell can only be predicted from the model when the cell is strongly pressurized (Vella et al., 2012; Sun and Paulose, 2021). However, the intragastric basal pressure is about 1.07 kPa after filling with a meal volume of 800 ml in healthy volunteers (Kwiatek et al., 2009), which is too low to be calculated from the pressurized shell indentation model.

For heterogeneous materials, such as an elastic layer of uniform thickness (gastric wall) overlaying another homogeneous material (pressurized gastric content), the indentation responses have been investigated from cells to large-scaled engineer systems using the bonded two-layer half-space indentation model (Dhaliwal and Rau, 1970; Staunton et al., 2016; Doss et al., 2019). Studies from different length scales showed the stiffnesses of the top layer, and the top layer wall thickness affect the indentation stiffness measurements significantly (Dhaliwal and Rau, 1970; Staunton et al., 2016; Doss et al., 2019). However, using the existing model to solve the indentation problems on heterogeneous materials, only the stiffness ratio between the top layer and the underlying material can be predicted.

This study aimed to build and verify a combined pressurized shell indentation model and the bonded two-layer half-space indentation model (the top wall layer and the bottom luminal contents wrapped by the wall) based on indentation tests on the stomach. The combined model was verified using a silicon stomach model, where the gastric wall properties and pressurized content stiffness as proxy for intragastric pressure during distensions were measured and estimated. We hypothesize that: 1) the gastric wall stiffness and pressurized gastric content stiffness can be estimated simultaneously by using the combined shell indentation model and the bonded two-layer indentation model from the stomach indentation tests; 2) the intragastric pressure is associated with the pressurized gastric content stiffness, and 3) the gastric wall stiffness and thickness affect the responses of the indentation test.

2. Material and methods

The below mechanical test on the gastric strips cut from the stomach model and indentation tests on the stomach model were done in two days in two locations (Aalborg University for mechanical tests and Aalborg University Hospital for indentation tests). For comparing the gastric wall stiffness obtained from the mechanical tests measurements to the indentation model calculation, the material properties of the stomach model should be stable and identical during the whole test period. Thus, a silicon stomach model was selected for this study in favor of an animal or human stomach.

2.1. Silicon stomach model

A one-layer silicon stomach model (1:1 ratio with the human stomach with a smooth outer surface and longitudinal rugae in the inner surface of the distal part of the stomach model) was used in this study (Ningbo Liuyedao Medical Treatment Technology Co., Ltd.). The silicon stomach model includes part of the lower esophagus and the upper duodenum (Fig. 1A).

2.2. Mechanical tests of the silicon stomach material

Three specimens (approximately 40 mm long, 10 mm wide, 5 mm thick) cut from the esophageal and duodenal ends of the stomach model were used for tensile tests. The tensile tests were performed on an INSTRON 2 kN testing system (6800 single column series 5944) at room temperature.

The specimen's wall thickness, width, and length between the two tensile grips were measured as the geometry parameters at the no-load state before the tensile test. Then the sample was stretched with a constant deformation rate (0.5 mm/s) until an elongation of 150%–200% of the initial length of the specimen was achieved. The tensile force and the elongation of the specimen were recorded for later tensile stiffness estimation.

2.3. Indentation test on the pressurized silicon stomach model

Before the indentation test, the middle line between the greater curvature and the lesser curvature of the stomach was marked. Four lines perpendicular to the middle line were drawn to distinguish the stomach model's proximal, middle-1, middle-2, and distal locations. The intersection points of the perpendicular and middle lines were the push force (indentation load) location, and the perpendicular lines were the scan paths of the ultrasonic probe in each stomach section (Fig. 1A).

2.3.1. Inflation of the stomach model

The silicon stomach model was submerged entirely in an organ bath filled with water at room temperature. After pressure equilibration, the duodenal end was closed via a connected cannula, and the esophageal end was connected via a tube to a water container. The container was used for applying static intragastric pressure ranging from 0 to 0.8 kPa. At each pressure step, equilibration was reached within a 5 min window (Fig. 1B).

2.3.2. Ultrasonographic measurements

The stomach was scanned using a B-mode 6 MHz ultrasonic probe (MylabTwice; Esaote, Italy). The probe was moved along the four perpendicular lines to scan the silicon stomach model, two cross-sectional images along each perpendicular line were captured and stored in BMP format for further off-line analysis (Fig. 1C). The probe was protected during the scanning using a latex-free sterile disposable probe cover; ultrasound conductive gel was utilized between the probe and the cover to allow a satisfactory sound wave propagation.

2.3.3. Indentation test

An electronic pressure algometer (Somedic Algometer Type II, SBMEDIC Electronics, Sweden) was used for the indentation test. The electronic display provides a pressure reading in kilopascals (kPa) and also displays the rate of applied pressure in a small LED window. The circular cylindric indenter having an area of 1 cm^2 was selected for the algometer in this study. The algometer was fixed on a retort stand with a ring clamp and a manipulator (ADInstruments, Oxford, UK). The algometer could be moved vertically up to 80 mm in 1 mm intervals by

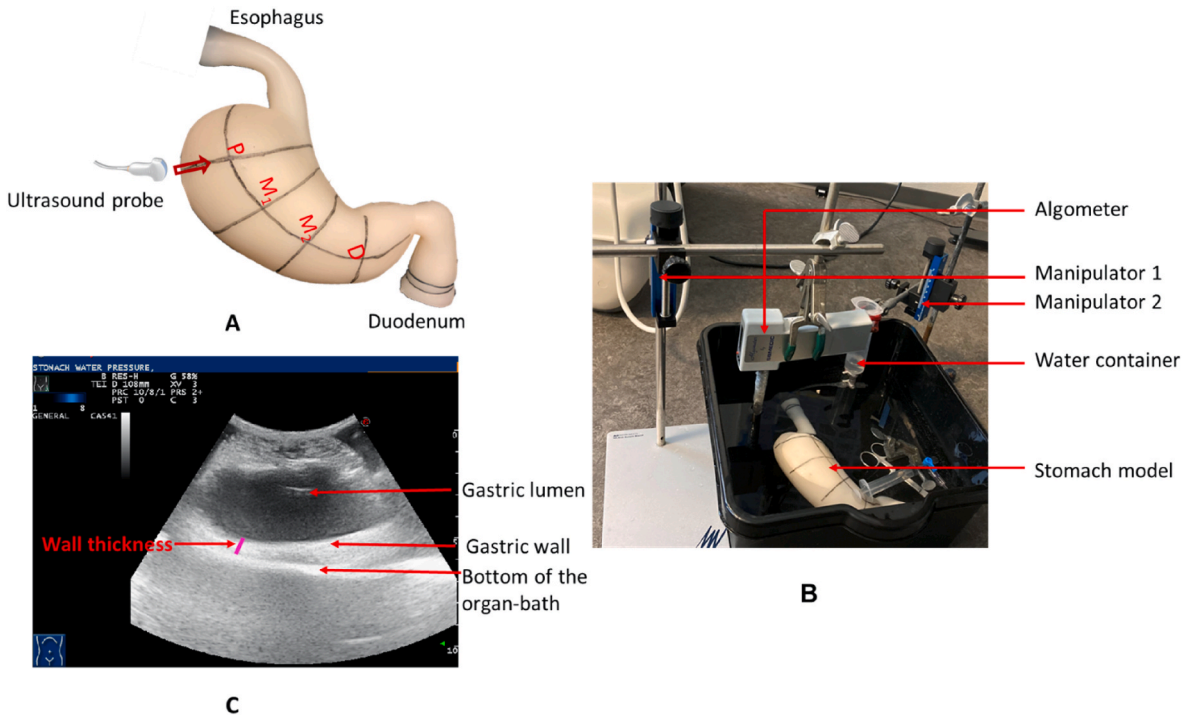

Fig. 1. Silicon stomach model and the test set up. **A:** The silicon stomach model 1:1 ratio with the human stomach. Four lines perpendicular to the middle line were used to distinguish the proximal (P), middle-1 (M1), middle-2 (M2), and distal (D) locations of the stomach model. The intersection points of the perpendicular and middle lines were the indentation loading points, and the perpendicular lines were the scan paths (the red arrow) of the ultrasonic probe in each stomach section. **B:** The indentation test and the stomach model inflation system, including the stomach model, a pressure algometer to conduct indentation force and two manipulators. One manipulator was used to control the indentation displacement by moving the algometer perpendicularly, and the other was used to control the intragastric pressure by adjusting the water level in the water container. **C:** A representative ultrasound image taken at pressure zero at the proximal location. The luminal cross-sectional area was identified semi-automatically for calculations of the inner radius. The wall thickness was obtained by averaging the five wall thickness measurements (the purple color line).

controlling the manipulator. The indenter was pushed perpendicularly at each marked loading point with depth from 0 to 30 mm in 2–5 mm intervals at each pressure level. The pushed depth was defined as the indentation displacement. The indentation displacements and the actual punctual pressure were read and recorded (Fig. 1B).

2.4. Data analyses

2.4.1. Tensile stiffness measurement

The tensile stiffness of the silicon stomach material was presented by the tensile Young's modulus, calculated from stress and strain curves obtained from the mechanical tests of the stomach material. The stress and strain were calculated as:

$$Stress: \quad \sigma = F/A_0 \tag{1}$$

Where F is the recorded force, and A_0 = thickness × width is the cross-sectional area of the specimen at the no-load state.

$$Stretch\ \ ratio: \quad \lambda = L_t/L_0 \tag{2}$$

Where L_t is the specimen's length during the stretch and L_0 is the length at the no-load state.

Strain ε is calculated as:

$$\varepsilon = \lambda - 1 \tag{3}$$

The apparent modulus of the elasticity was used to present the tensile stiffness E_T in this study with an assumption of a linear stress-strain relationship when $\varepsilon < 1.0$, as:

$$E_T = \sigma/\varepsilon \tag{4}$$

2.4.2. Ultrasound image processing

Ultrasound images in BMP format were exported with image resolutions from 0.25 to 0.34 mm per pixel. The images were processed using a custom-made MATLAB program (R2020B, The MathWorks, Inc.). The inner outlines of the cross-section of the stomach model were visually identified, and the luminal cross-sectional area (CSA) was calculated. The gastric wall thickness was measured five times in locations where the stomach model touched the bottom of the organ bath (Fig. 1C).

The inner radius of the cross-section at the intragastric pressure p is: $R(p) = \sqrt{CSA_{luminal}(p)/\pi}$, the $CSA_{luminal}(p)$ is the luminal CSA of the stomach model.

The stomach model wall thickness at the intragastric pressure p, $h(p)$ was obtained by averaging the five measured wall thicknesses in each cross-sectional image.

2.4.3. Indentation stiffness

The indentation force was calculated by multiplying the actual push pressure by the indenter area (1 cm^2 in this study). At each pressure, the indentation force-displacement relationship was assumed linear, and the indentation stiffness at each indentation loading point *ks(p)* was the slope of the linear curve fitted to the indentation force-displacement curves as:

$$FI(p) = ks(p)*\delta(p) + b(p) \tag{5}$$

Where *FI(p)* is the indentation force, *δ(p)* is the indentation displacement, *b(p)* is a constant, and p is the intragastric pressure.

2.4.4. The gastric stiffness estimated from the homogeneous gastric model

In the homogeneous gastric model, we assumed the stomach model, including the gastric wall and the gastric content as a homogeneous and

isotropic material. By conducting the indentation test, the elastic stiffness of the stomach model can be estimated by fitting the indentation force-displacement curve to the model of the contact between a rigid cylinder with a flat end and an elastic half-space (Sneddon, 1965) as (Fig. 2A):

$$FI(p) = 2a\frac{E(p)\delta(p)}{(1-\nu^2)} \tag{6}$$

Where a is the contact radius between the indenter and the silicon stomach model, in this study, the indenter size was 1.0 cm^2, so $a = \sqrt{(1.0/\pi)} = 0.564cm$. ν is Possion's ratio, in this study, $\nu = 0.49$ for silicon rubber was selected for the stomach model (Wolf and Descamps, 2002; Mott et al., 2008), $E(p)$ is the elastic stiffness of the stomach model, and it increased in function with the intragastric pressure increase. With the measured indentation force and displacement, the $E(p)$ can be obtained by linear curve fitting Eq. (6) to the indentation force and displacement curves.

2.4.5. The gastric wall and content stiffness estimated from the heterogeneous gastric model

In the above-mentioned homogeneous gastric model analysis, the mechanical properties of the gastric wall and gastric content were assumed to be identical, and the gastric wall thickness's effect on gastric stiffness was not considered. In the heterogeneous gastric model, we assumed the gastric model consists of the linear elastic gastric wall and the pressurized gastric contents wrapped by the gastric wall. The gastric wall stiffness was considered to be a constant during the distension, while the gastric content stiffness changed with the distension pressure of the stomach. The gastric wall stiffness was estimated from the shell indentation models at zero pressure state. The stomach content stiffness under the pressurized states was calculated using the indentation model on a bonded two-layer elastic half-space (Fig. 2B).

2.4.5.1. Stiffness estimation of the gastric wall based on indentation shell model. We assumed that the gastric wall stiffness was identic for all gastric sections. Hence, the indentation test at the proximal stomach section was used to calculate the wall stiffness in this study. The proximal stomach was assumed as a spheroidal shell. The calculated inner radius of the cross-sections and the wall thickness of the proximal stomach at zero pressures were used in the analysis.

When an indentation acts on a point along the equator of the spheroidal shell, the indentation stiffness at zero-pressure $ks(0)$ can be denoted as (Sun and Paulose, 2021):

$$\mathrm{ks}(0) = 8\sqrt{\kappa_0 * \mathrm{Y}_0 * KG_0} \tag{7}$$

Where $\kappa_0 = \frac{\mathrm{E}_1 * \mathrm{h}(0)^3}{12*(1-\nu_1^2)}$ is the bending stiffness at $p = 0$, $h(0)$ is the gastric wall thickness at $p = 0$, $\nu_1 = 0.49$ is the Poisson's ratio for the gastric wall, E_1 is the gastric wall stiffness, $\mathrm{Y}_0 = \mathrm{E}_1 * \mathrm{h}(0)$, $\mathrm{KG}_0 := \frac{1}{R_{x0}R_{y0}}$ is the Gaussian curvature at $p = 0$, R_{x0}, and R_{y0} are the principal radii of curvature of the spheroidal shell along x- and y- orientations at $p = 0$, respectively. As the proximal stomach was assumed as a spheroidal shell, thus $R_{y0} = R_{x0} = R(0)$, that were measured from the ultrasound images at $p = 0$. Hence, the gastric wall stiffness E_1 of the proximal stomach can be obtained from Eq. (7) using the measured indentation stiffness at $p = 0$ as:

$$\mathrm{E}_1 = \sqrt{\mathrm{ks}(0)^2 * 12 * (1-\nu_1{}^2) / \left(64\mathrm{KG}_0 * \mathrm{h}(0)^4\right)} \tag{8}$$

2.4.5.2. Pressurized gastric content stiffness. As shown in Fig. 2B, the top layer is the gastric wall with the wall stiffness E_1, Poisson's ratio ν_1, and the bottom substrate layer is the gastric content during the pressurization with stiffness E_2, Poisson's ratio ν_2, and is presumed to be infinitely thick. The gastric wall stiffness E_1 was estimated from Eq. (8) with the known indentation stiffness, the wall thickness, and the luminal radius of curvature at a zero-pressure state. To analyze the indentation model on the heterogeneous materials, Dhaliwal and Rau presented a generalized analytical solution to the indentation problem of two bonded layers with different elastic properties (Dhaliwal and Rau, 1970) (Fig. 2B) in the form of a Fredholm Integral Equation of the Second Kind (Atkinson and Shampine, 2008; Staunton et al., 2016; Doss et al., 2019) (see Eqs. (A.1)-(A.9) in the appendix). The equations can be solved, and the indentation force can be expressed theoretically in terms of the indenter shape, the stiffness and Poisson's ratios of the gastric wall and the pressurized gastric content (E_1, E_2, ν_1, ν_2), the thickness of the gastric wall $h(p)$, and the indentation displacement $\delta(p)$. This study used the circular cylindric indenter with an indenter area of 1.0 cm^2. The Poisson's ratio of the gastric wall is $\nu_1 = 0.49$, and the fluid-like chyme in the gastric lumen was assumed nearly incompressible with Poisson's ratio $\nu_2 = 0.49$. The gastric wall stiffness E_1 obtained from Eq. (8) were assumed constant during the pressurization. The only unknown parameter E_2, i.e., the gastric content stiffness under pressurization state, can thus be obtained by curve fitting the theoretical indentation force function to the measured indentation force-displacement curve (see Eqs. (A.10)-(A.12) in the appendix).

2.5. Statistical analysis

Data are presented as mean ± SD. Independent-samples t-test was used to compare the luminal radius and wall thickness between zero pressure and pressure 0.8 kPa. The gastric wall elastic stiffness measured

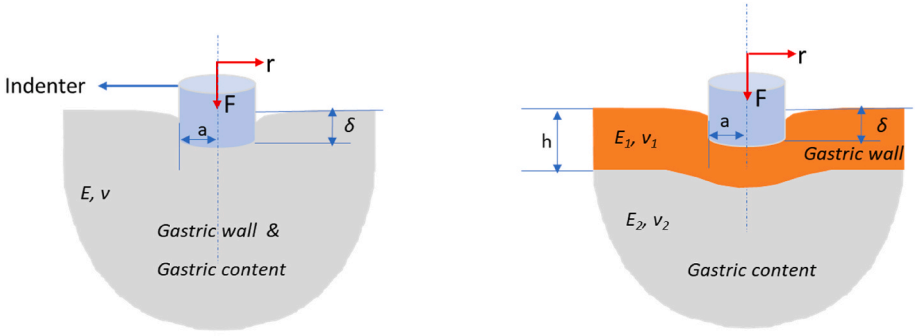

Fig. 2. Schematic diagram of the axisymmetric indentations by a flat-ended rigid cylinder on **A**: a homogeneous elastic half-space, and **B**: a gastric wall layer bonded to an elastic substrate, i.e., gastric content. F: indentation force, r: radial direction of the axisymmetric system, δ: indentation displacement, a: indenter radius, E, ν: the elastic stiffness and the Poisson's ratio of the homogeneous stomach model, h: the gastric wall thickness, E_1, ν_1: the elastic stiffness and the Poisson's ratio of the gastric wall, E_2, ν_2: the elastic stiffness and the Poisson's ratio of the gastric content in pressurized states.

from the tensile test and calculated from the shell model were compared using the *t*-test. One-way analysis of variance (ANOVA) with repeated measures was used to compare the indentation stiffness, gastric stiffness obtained from the homogeneous model, and the pressurized gastric content stiffness obtained from the bonded two-layered heterogeneous model in different locations of the gastric model at each pressure step. Correlations between the calculated pressurized gastric content stiffness and the intragastric pressure were performed with the Pearson correlation. $p < 0.05$ was considered statistically significant. All analyses were done with the IBM SPSS Statistics (IBM Corp, Version 27).

3. Results

3.1. Tensile stiffness of the stomach material

The thickness and width of the strips cut from the stomach model were 4.9 ± 0.4 mm and 10.0 ± 0.4 mm, respectively. The tensile stress-strain curves for the three samples are shown in Fig. 3. The averaged tensile stiffness from the tensile tests of the three samples is 38.7 ± 6.7 kPa.

3.2. Ultrasound measurements

The measured cross-sectional area, the gastric wall thickness, and the calculated luminal radius for the proximal, middle-1, middle-2, and distal locations of the gastric model in pressures from 0 to 0.8 kPa are shown in Table 1. It shows the luminal radii tended to increase, and the wall thickness tended to decrease in all four locations at pressure 0.8 kPa compared to the configurations at pressure 0 kPa. However, the statistical significance was only found for the luminal radius in the middle 1 ($p = 0.002$) and the wall thickness in the proximal ($p = 0.04$) locations.

3.3. Indentation stiffness of the stomach model

The indentation force and displacement relationship at the proximal, middle-1, middle-2, and distal locations are shown in Fig. 4. The indentation stiffness obtained by linear curve fitting the indentation force and displacement curves is shown in Table 2. In comparison to other locations, the indentation stiffness at the middle-1 was the highest in all pressure levels ($p < 0.002$), and there was no difference in the indentation stiffness among the other three locations (all $p > 0.07$).

3.4. Gastric wall and content stiffness estimated from the homogeneous gastric model

With the indentation force and indentation displacement relationships presented in Fig. 4, the gastric wall and content stiffness was calculated from Eq. (6). The calculated gastric wall and content stiffness

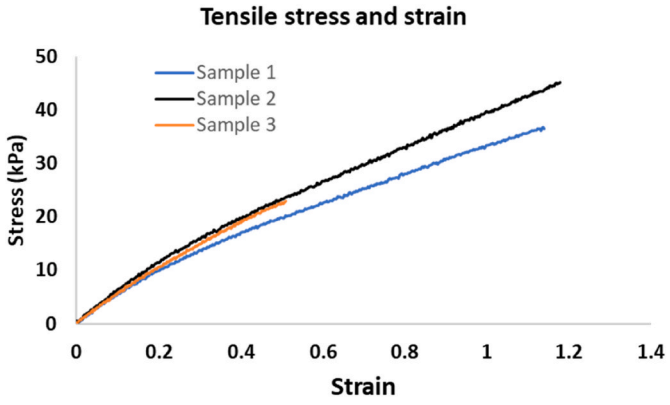

Fig. 3. Tensile stress-strain curves obtained from the mechanical tensile tests on three samples.

Table 1
Morphometric data of the stomach model.

Intragastric pressure (kPa)		0	0.2	0.4	0.6	0.8
proximal	CSA (mm^2)	2486 ± 326	2983 ± 255	2925 ± 136	2946 ± 111	3114 ± 299
	Radius (mm)	28.1 ± 1.8	30.8 ± 1.3	30.5 ± 0.7	30.6 ± 0.6	31.4 ± 1.5
	Thickness (mm)	5.8 ± 0.3	5.9 ± 0.2	5.8 ± 0.1	5.2 ± 0.1	4.5 ± 0.5
middle-1	CSA (mm^2)	2025 ± 32	2516 ± 236	2511 ± 186	2820 ± 109	2823 ± 92
	Radius (mm)	25.4 ± 0.2	28.3 ± 1.3	28.3 ± 1.0	29.9 ± 0.5	30.0 ± 0.4
	Thickness (mm)	6.9 ± 0.5	7.1 ± 0.8	6.4 ± 0.1	6.6 ± 0.4	6.0 ± 0.1
middle-2	CSA (mm^2)	1382 ± 234	1632 ± 287	1420 ± 120	1687 ± 210	1889 ± 224
	Radius (mm)	20.9 ± 1.8	22.7 ± 2.0	21.2 ± 0.9	23.1 ± 1.4	24.5 ± 1.5
	Thickness (mm)	6.1 ± 0.9	7.0 ± 0.4	6.5 ± 0.1	6.3 ± 0.8	5.4 ± 0.5
distal	CSA (mm^2)	1061 ± 147	1031 ± 101	974 ± 294	1030 ± 226	1189 ± 131
	Radius (mm)	18.3 ± 1.2	18.1 ± 0.9	17.4 ± 2.5	18.0 ± 2.0	19.4 ± 1.1
	Thickness (mm)	6.6 ± 1.2	6.6 ± 0.7	6.9 ± 0.5	6.0 ± 0.3	6.1 ± 1.2

Notes: Data are presented as mean ± SD, CSA: cross-sectional area.

and its relationship to the intragastric pressure in the proximal, middle-1, middle-2, and distal locations are shown in Fig. 5. It shows the gastric wall and content stiffness increased with the distension pressure for all four locations, and the stiffness at the middle-1 location was the highest for all distension pressures ($p < 0.001$).

3.5. Gastric stiffness estimated from the heterogeneous gastric model

3.5.1. Gastric wall stiffness

The gastric wall stiffness estimated from Eq. (8) in the proximal stomach at zero-pressure was 30.1 ± 5.6 kPa. The estimated gastric wall stiffness had no difference from the tensile stiffness measured by the mechanical tensile test on the strips cut from the stomach model ($p = 0.14$).

3.5.2. Pressurized gastric content stiffness

With a known indentation displacement, the indentation force can be calculated from Eq.(A.10). The representative experimental recorded and theoretical calculated indentation force-displacement curves are shown in Fig. 6A. It shows that the theoretical calculations align with the experimental recordings. The maximum root mean square of the fitting error between the theoretical calculations and the experimental recordings was 0.097. The estimated gastric content stiffness at the proximal, middle-1, middle-2, and distal locations in functions of the intragastric pressure are shown in Fig. 6B. The gastric content stiffness was strongly associated with the intragastric pressure for all four locations ($r > 0.83$ and $p < 0.001$). For each distension pressure, the calculated gastric content stiffness in the proximal and middle-1 locations was higher than that at the middle-2 and distal locations ($p < 0.001$), but there is no difference in the stiffness between the proximal and the middle-1 locations ($p = 0.58$). In comparison to the gastric wall and content stiffness calculated from the homogeneous gastric model, the pressurized gastric content stiffness was significantly lower for all four locations in all distension pressures ($p < 0.001$).

4. Discussion

This in-vitro/silicon model study calculated the gastric wall stiffness and pressurized gastric content stiffness simultaneously by combining

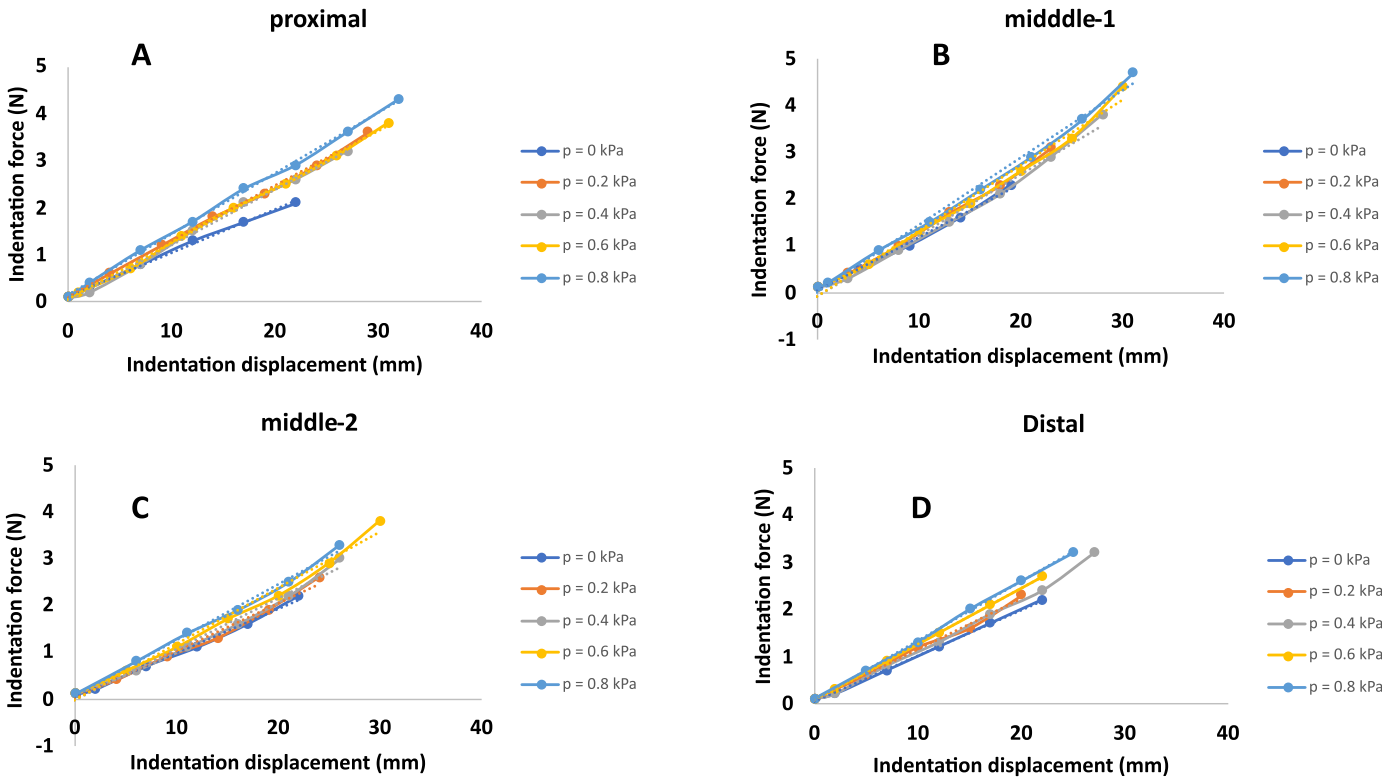

Fig. 4. The measured indentation force-displacement curves for the proximal (A), middle-1 (B), middle-2(C) and distal (D) locations at the intragastric pressures 0, 0.2, 0.4, 0.6, and 0.8 kPa. For all four locations, the curves from pressure 0.8 kPa presented on top of the other curves, indicating the increased indentation stiffness at the pressure 0.8 kPa compared to the curves from the lower pressures. The solid lines with solid circulars are the measured data, and the dotted lines are the linear function fitted curves; the slopes of the linear function is the indentation stiffness presented in Table 2.

Table 2
Indentation stiffness of the stomach model.

Intragastric pressure (kPa)	proximal (kN.m^{-1})	middle-1 (kN.m^{-1})	middle-2 (kN.m^{-1})	distal (kN.m^{-1})
0	0.092	0.115	0.095	0.097
0.2	0.118	0.13	0.103	0.108
0.4	0.118	0.131	0.11	0.113
0.6	0.118	0.140	0.120	0.119
0.8	0.129	0.144	0.120	0.125

the advanced shell indentation model and the bonded two-layer (the top wall layer and the bottom luminal contents wrapped by the wall) half-space indentation model. The stiffness estimation was based on concurrent non-invasive indentation test on the silicon stomach model with ultrasound measurements of the dimensions of the stomach model. The calculated gastric wall stiffness fits well with the tensile stiffness measured by the tensile test, and the calculated pressurized gastric content stiffness was strongly associated with the intragastric pressure. To the best of our knowledge, this is the first study that used the combined shell indentation model and the bonded two-layer indentation

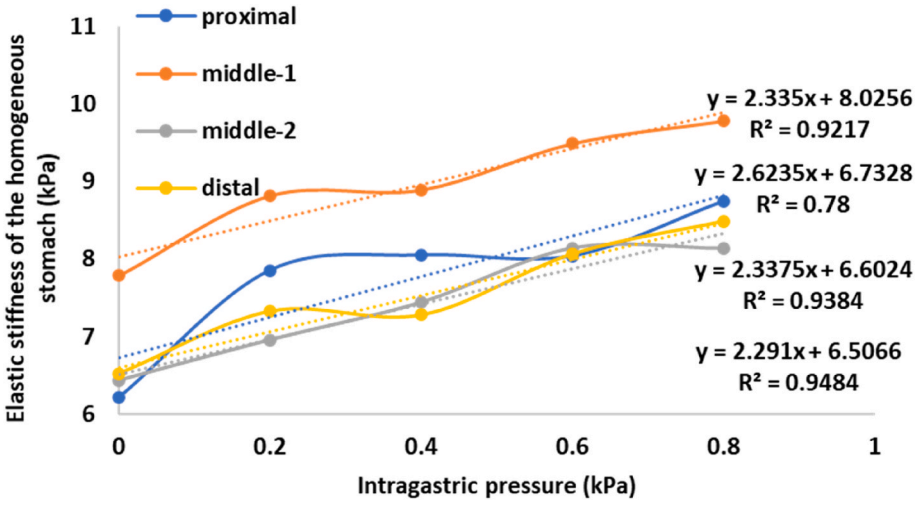

Fig. 5. The elastic stiffness of the homogeneous stomach model in relation to the intragastric pressure. The stiffness in the middle-1 location was significantly higher than the stiffness in other locations for all distension pressures.

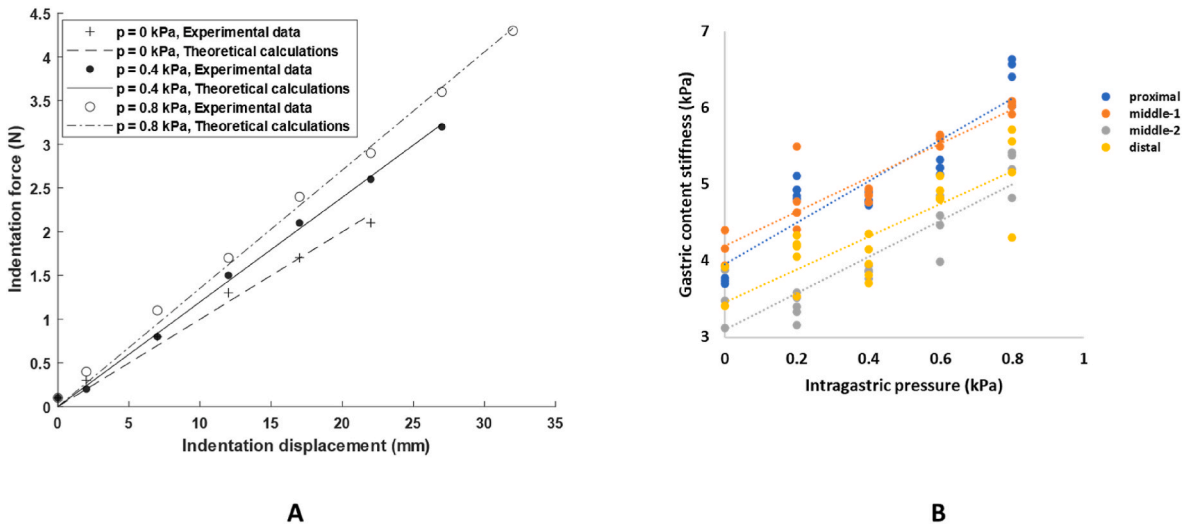

Fig. 6. The calculations from the bonded two-layer gastric model. **A:** Representative indentation force-displacement experimental data (scatters) and the theoretical calculations by using the analytical indentation model of the bonded two-layer linear elastic materials (lines) from the proximal stomach in pressure 0, 0.4 and 0.8 kPa. **B:** The gastric content stiffness change as a function of the intragastric pressure in all four locations in the stomach model. The gastric content stiffness was obtained by the theoretical indentation analysis on the bonded two-layer model and the known gastric wall elastic stiffness calculated from the shell theory at the zero intragastric pressure.

model to quantitatively estimate the wall and pressurized content stiffness in an in-vitro/silicon stomach model. The method can be applied in future clinical studies to investigate the intragastric pressure conditions non-invasively via the pressurized gastric content stiffness with concurrent non-invasive abdominal indentation tests and medical imaging technologies, such as magnetic resonance imaging (MRI).

4.1. Methodological aspects

Compared to current existing non-invasive intra-visceral pressure measurement techniques, i.e., IAP measurements (Van Ramshorst et al., 2011; Tang et al., 2021; Tayebi et al., 2021), the current modelling analysis is superior in estimating the luminal content stiffness changes with the intraluminal pressure by taking the wall effect into the calculation. Previous non-invasive IAP measurements were based on the indentation stiffness measurement of the abdominal wall, and the abdominal cavity was considered a cylindrical structure filled with isotropic homogeneous content. Our analysis showed that gastric wall stiffness and thickness significantly affect the stiffness estimation of the gastric content. The gastric wall and content stiffness estimated from the homogeneous model (Fig. 5) were significantly higher than that from the bonded two-layer model (Fig. 6). The stiffness change was discontinuous from proximal to middle-1 and middle-2 locations, represented by a sudden higher stiffness in the middle-1 location compared to the proximal and middle-2 parts of the stomach model. Our modelling analysis showed that the gastric wall elastic stiffness was about five-fold higher than the gastric content stiffness even at the distension pressure of 0.8 kPa (approximate the intragastric pressure on filling volume 400 ml (Kwiatek et al., 2009)). Hence, the stiffness obtained from the homogeneous model might not be directly related to the intragastric pressure as the gastric wall properties were simplified as an identical matter to the gastric content. The thicker wall in the middle-1 location could be a major factor that attributes to the higher indentation stiffness and thus the higher gastric wall and content elastic stiffness at the middle-1 location in the homogeneous gastric model. In contrast, the gastric content stiffness estimated from the bonded two-layer model showed a similar stiffness distribution between the proximal and middle-1 locations and between the middle-2 and distal locations. Hence, the wall effect, including wall thickness and stiffness, must be considered during the intragastric pressure estimation. The smaller indentation stiffness and the elastic stiffness of the gastric content in the middle-2 and distal parts of the stomach could be caused by the folds in the inner surface of the stomach model. The silicon stomach mimics the human stomach anatomy with longitudinal rugae in the inner surface of the distal part of the stomach model. The longitudinal folds could be a reason for the thicker wall, lower indentation stiffness, and lower gastric content stiffness in the distal part of the stomach. Future studies using enhanced ultrasound imaging or MRI with improved image resolutions should be performed to precisely distinguish the inner surface folds and the wall thickness measurement.

4.2. Clinical aspects

Gastric accommodation describes the reduction in gastric tone and increase in compliance that follows ingestion of a meal. It can be documented with several techniques including the barostat/tensostat as the gold standard (Kay and Jørgensen, 1994; Kindt and Tack, 2006), as well as other existing imaging methods such as ultrasound or MRI (Kim and Camilleri, 2002; Janssen et al., 2011; Banerjee et al., 2020). Among these technologies, the barostat/tensostat is the only one that can simultaneously measure the intragastric pressure and compliance during the accommodation. Detailed biomechanical/physiological evaluations of gastric accommodation require simultaneous assessment of gastric volume and the intragastric pressure change during food intake. Previous barostat studies have shown that people with impaired gastric accommodation had higher intragastric pressure during volume-controlled balloon distensions in the proximal stomach, indicating an increased gastric wall stiffness (Piessevaux et al., 2001). However, barostat/tensostat studies are invasive, perceived as uncomfortable and stressful, and normally not part of routine clinical practice application.

Barostat/tensostat studies suggested that it is the tension of the stomach wall, rather than the elongation as the origin of the transmission of proprioceptive signals from the proximal stomach, meaning that the gastric satiation signals originate from the combination of the intragastric pressure and wall's geometric change (Cummings and Overduin, 2007). The wall tension can be approximated using the simplified law of Laplace as Tension = intragastric pressure/(2*mean curvature), where the curvatures are variables used to characterize the local shape of the gastric surface. In this study, the curvature of the

proximal stomach was calculated using transversal ultrasound images of the stomach. The intragastric pressure can be estimated from the linear correlations between the elastic stiffness of the gastric content and the intragastric pressure. Hence, the gastric tension during gastric distension can only be obtained from the invasive Barostat/tensostat test being calculated from the current modelling analysis with the non-invasive indentation tests.

4.3. Limitations of the study

We used a silicon one-layer homogeneous stomach model as an initial start to investigate the non-invasive measurements of gastric wall stiffness and intragastric pressure. In this study, the gastric wall stiffness analysis was obtained from a spheroidal shell indentation model calculation, where the proximal stomach was assumed as a spherical shape. The stomach is a hollow organ with an irregular geometric shape, and although the proximal stomach has been assumed as spherical in several studies (Azpiroz and Malagelada, 1987), this could be a source of errors in the calculation of the gastric wall stiffness between the modelling analysis and the mechanical tensile test.

In the present study, we used a silicon stomach model to estimate the gastric wall stiffness using the shell indentation model with the ultrasound images of the proximal stomach model at zero pressure. Although the feasibility of assessing the proximal gastric accommodation on the ultrasound images have been confirmed by several studies (Undeland et al., 1998; Olafsdottir et al., 2000; Tefera et al., 2001; Fan et al., 2013), it is very difficult to carry out indentation test on the proximal stomach from the scanning locations due to their anatomical locations in the body. On the other hand, the antrum and, more generally, the distal section of the stomach is usually the easiest to visualize by ultrasound (Steinsvik et al., 2021) while also being a suitable place for abdominal indentation tests. With the simultaneous ultrasound scanning, the locations where the stomach wall contacts the abdominal wall can be identified as the push force (indentation load) location for the abdominal indentation test. By passing the recorded indentation force, indentation displacement, and the measured stomach configuration into the models presented in this study, the gastric stiffness as a proxy to the intragastric pressure can thus be calculated. However, to estimate the gastric wall stiffness from indentation tests on the distal locations, we need to reshape the calculation model from the current spheroidal shell geometry to an ellipsoid one to reduce the errors caused by geometrical differences between proximal and distal parts of the stomach. This study was limited to scanning the cross-sectional images along the transversal axis of the stomach model due to 2D ultrasound images. Hence, the ellipsoid model was not considered in this study, and it could be derived by using 3D ultrasound scanning or MR scanning in future studies.

By assuming a linear gastric wall mechanical property, this study selected a silicon stomach model to test and verify the combined pressurized shell indentation model and the bonded two-layer half-space indentation model. Previous biomechanical studies on the animal (Zhao et al., 2008) and human (Toniolo et al., 2022) stomach showed nonlinear stress-strain curves of the stomach tissue. According to a recent study done by Toniolo and co-workers, the nonlinear stress-strain relationship of the stomach tissues can be simplified using bi-linear functions, i.e, two different linear stress-strain relationships for toe- and quasi-linear regions, respectively (Toniolo et al., 2022). Toniolo's study proved the stress-strain curves from all stomach regions could be assumed as a linear function in the strain range 0–0.8. The multi-scale stomach mechano-physiological modelling analysis from Akhmadeev et al. showed that the maximum stretch ratio was 1.35 in the fundus area under an intragastric pressure of 20 kPa (Akhmadeev and Miftahof, 2010). That is much higher than the physiological intragastric pressure measured by Kwiatk et al. (1.07 kPa at a meal volume of 800 ml (Kwiatek et al., 2009),). The maximum intragastric pressure used in this study was 0.8 kPa, far below the pressure used in Akhmadeev's model. Hence the maximum strain of the stomach during the distension in this study should be lesser than 0.8. It is therefore reasonable to assume the linear stress-strain relationship of the stomach in this study. However, to accurately evaluate how the material nonlinearity of the human stomach affect the model result, the future numerical models with different material properties need to be compared.

Because of the relatively lower physiological intragastric pressure (1.07 kPa in meal volume 800 ml (Kwiatek et al., 2009)) in comparison to the turgor pressures in, such as yeast cells (100–200 kPa (Vella et al., 2012)), the pressurized shell indentation models used for transmural pressure estimation in cells (Vella et al., 2012; Sun and Paulose, 2021) can not be used for indentation tests of the stomach. Hence the gastric content stiffness rather than the intragastric pressure was calculated from the modelling analysis in this study. This study showed the gastric content stiffness is strongly associated with the intragastric pressure. The gastric content stiffness can be used as a proxy to infer the intragastric pressure and reveal the intragastric pressure conditions during gastric accommodation and emptying. For assessing the absolute value of the intragastric pressure from the abdominal indentation test, a developed indentation stomach shell model or numerical simulations of the indentation responses need to be considered in future stomach indentation studies.

In our study, the pressure algometer and a manipulator system used to control the indentation displacement were complex and not portable. However, some portable tensiometer devices have been shown in the literature (Tang et al., 2021; Tayebi et al., 2021), but unfortunately, they have not yet been commercialized and cannot be found on the market yet. This limitation could be overcome in the future by developing a portable MR environment-friendly tensiometer combined with force, displacement transducers to approach a comprehensive solution.

In our study, all the tests and analyses were performed on a silicon stomach model. During the model analysis, the surrounding tissue effects, including the abdominal wall, intra-abdominal pressure outside the stomach, displacement of the entire stomach during trans-abdominal indentation, were not taken into account. Future validation tests in human studies must be carried out to interpret the clinical translation of the developed analyses.

4.4. Conclusions and perspectives

In conclusion, the proposed non-invasive indentation assessment approach and mechanical modelling analysis are feasible and can distinguish between gastric wall stiffness and pressurized gastric content stiffness. The obtained gastric content stiffness correlated with intragastric pressure significantly and can be used as a proxy of the intragastric pressure. The measurement and analysis have the potential to be further developed into a diagnostic system to investigate gastric function/dysfunction in clinical practice via the estimated gastric wall stiffness and the gastric content stiffness with concurrent non-invasive abdominal indentation tests and medical imaging technologies. However, as a new method, the indentation measurement and modelling analysis must be further validated and standardized on a human model for a more reliable and reproducible assessment, which is required for translations to the clinical practice.

Funding

This article was supported by Aage og Johanne Louis-Hansens Fond, Denmark (22-2B-10079) and A.P. Møller Fonden, Denmark (L-2021-00034). The funders had no role in study design, data collection and analysis, decision to publish, or preparation of the manuscript.

CRediT authorship contribution statement

Donghua Liao: Writing – review & editing, Writing – original draft, Methodology, Investigation, Funding acquisition, Formal analysis, Data curation, Conceptualization. **Esben Bolvig Mark:** Writing – review &

editing, Writing – original draft, Funding acquisition, Conceptualization. **Rasmus Bach Nedergaard:** Writing – review & editing, Writing – original draft, Conceptualization. **Lars Rosgaard Jensen:** Writing – review & editing, Investigation. **Davide Bertoli:** Writing – review & editing, Investigation. **Jens Brøndum Frøkjær:** Writing – review & editing, Resources, Conceptualization. **Donghong Yu:** Writing – review & editing, Resources, Methodology. **Jingbo Zhao:** Writing – review & editing, Resources, Methodology. **Christina Brock:** Writing – review & editing, Resources, Conceptualization. **Asbjørn Mohr Drewes:** Writing – review & editing, Supervision, Resources, Conceptualization.

Declaration of competing interest

The authors declare that they have no known competing financial interests or personal relationships that could have appeared to influence the work reported in this paper.

Data availability

Data will be made available on request.

Appendix

Analytical indentation model of the bonded two-layer linear elastic materials

Dhaliwal and Rau presented a generalized analytical solution to the indentation problem of two bonded layers in the form of a Fredholm Integral Equation of the Second Kind as [A1]:

$$\varphi(\mathrm{t}) + \frac{\mathrm{a}}{h\pi}\int_0^1 \mathrm{K}(\mathrm{x},\mathrm{t})\varphi(\mathrm{x})\,\mathrm{dx} = -\frac{\mathrm{E_1 a}}{2(1-\nu_1^2)}\,(\delta - \beta(\mathrm{t})) \tag{A.1}$$

$$\mathrm{F} = -4\int_0^1 \varphi(\mathrm{t})\,\mathrm{dt} \tag{A.2}$$

$$\varphi(1) = 0 \tag{A.3}$$

Where a is the contact radius between the indenter and the silicon stomach model, in this study, the indenter size was 1.0 cm^2, so $a = \sqrt{(1/\pi)}^* 10 = 5.64$ mm. δ is the indentation displacement, h is the gastric wall thickness, E_1 and ν_1 are the stiffness and the Poisson's ratio of the gastric wall, F is the indentation force, and β(t) is the function that related to indenter shape. In this study, the flat-ended cylindrical indenter was used, thus

$$\beta(\mathrm{t}) = 0 \tag{A.4}$$

Here $\varphi(t)$ is an intermediate function related to the stress profile of the indentation, and the kernel K is smooth and defined by:

$$\mathrm{K}(\mathrm{x},\mathrm{t}) = 2\int_0^\infty \mathrm{H}(2\mu)\cos\left(\frac{\mathrm{a}}{\mathrm{h}}t\mu\right)\cos\left(\frac{\mathrm{a}}{\mathrm{h}}x\mu\right)\,d\mu \tag{A.5}$$

with

$$\mathrm{H}(\mu) = -\frac{\mathrm{d} + \mathrm{g}(1+\mu)^2 + 2\mathrm{dge}^{-\mu}}{\mathrm{e}^{\mu} + \mathrm{d} + \mathrm{g}(1+\mu^2) + \mathrm{dge}^{-\mu}} \tag{A.6}$$

$$\mathrm{d} = \frac{(3-4\nu_1) - \mu(3-4\nu_2)}{1+\mu(3-4\nu_2)} \tag{A.7}$$

$$g = \frac{1-\mu}{\mu + 3 - 4\nu_1} \tag{A.8}$$

$$\mu = \frac{E_1(1+\nu_2)}{E_2(1+\nu_1)} \tag{A.9}$$

Where E_2 and ν_2 are the stiffness and the Poisson's ratio of the pressurized gastric content. The function φ in Eq. (A.1) can be solved numerically in MATLAB using the program Fie developed by Atkinson et al. [A2], then the indentation force can be calculated using Eq. (A.2). The indentation force F at the pressurized state in Eq.(A.2) is a function of the indenter radius $a = 5.64$ mm, the stiffness and Poisson's ratios of the gastric wall and the pressurized gastric content ($E_1 = 30.1 \pm 5.6$ kPa, E_2, $\nu_1 = \nu_2 = 0.49$), the ultrasound measured gastric wall thickness h, and the indentation displacement δ. They can be expressed by J_p as:

$$F = J_p(a, E_1, E_2, \nu_1, \nu_2, h, \delta) \tag{A.10}$$

For each distension pressure, a, E_1, ν_1 and ν_2 are constants, the gastric wall thickness h was measured from the ultrasonic images. Hence, the pressurized gastric content stiffness E_2 can be determined using a nonlinear least-squares (Levenberg-Marquardt) minimization of the difference

between computed and measured indentation force pressures during the indentation displacement. The integral function in Eq.(A.2) was numerically approximated, i.e., the following objective function was minimized:

$$S(A) = \sum_{i=1}^{m} \left[J_p(a, E_1\ E_2, \nu_1, \nu_2, h, \delta) - \mathrm{F}_i \right]^2 = min \tag{A.11}$$

where m is the number of data points, J_p is the computed indentation force from Eq. (A.2), and F_i *is* the measured indentation force. The unknown material parameter E_2 was obtained by fitting the model to the recorded indentation force-displacement curves of the stomach model. As a metric of the goodness of fit, we computed the root mean square of the fitting error:

$$RMSE = \sqrt{\frac{S(A)}{m}} \tag{A.12}$$

All calculations were optimized using MATLAB subroutines (R2020, Mathworks, USA).

[A1] R. S. Dhaliwal and I. S. Rau, "Axisymmatric Boussinesq problem for a thick elastic layer under a punch of arbitraty profile.," Int. J. Engng. Sci., vol. 8, pp. 843–856, 1970, [Online]. Available: https://doi.org/10.1016/j.ifacol.2016.11.148.

[A2] K. E. Atkinson and L. F. Shampine, "Algorithm 876: Solving Fredholm Integral Equations of the Second Kind in Matlab," ACM Trans. Math. Softw., vol. 34, no. 4, Jul. 2008, https://doi.org/10.1145/1377596.1377601.

References

Akhmadeev, N.R., Miftahof, R., 2010. Stress-strain distribution in the human stomach. Int. J. Des. Nat. Ecodyn. 5 (2), 90–107. https://doi.org/10.2495/DNE-V5-N2-90-107.

Atkinson, K.E., Shampine, L.F., 2008. Algorithm 876: solving Fredholm integral equations of the Second Kind in Matlab. ACM Trans. Math Software 34 (4). https://doi.org/10.1145/1377596.1377601.

Azpiroz, F., Malagelada, J.R., 1987. Gastric tone measured by an electronic barostat in health arid postsurgical gastroparesis. Gastroenterology 92 (4), 934–943. https://doi.org/10.1016/0016-5085(87)90967-X.

Banerjee, S., Pal, A., Fox, M., 2020. Volume and position change of the stomach during gastric accommodation and emptying: a detailed three-dimensional morphological analysis based on MRI. Neuro Gastroenterol. Motil. 32 (8), 1–14. https://doi.org/10.1111/nmo.13865.

Cummings, D.E., Overduin, J., 2007. Gastrointestinal regulation of food intake. J. Clin. Invest. 117 (1), 13–23. https://doi.org/10.1172/JCI30227.

Dhaliwal, R.S., Rau, I.S., 1970. Axisymmatric Boussinesq problem for a thick elastic layer under a punch of arbitraty profile. Int. J. Eng. Sci. 8, 843–856. https://doi.org/10.1016/j.ifacol.2016.11.148. Available at:

Distrutti, E., et al., 1999. Gastric wall tension determines perception of gastric distention. Gastroenterology 116 (5), 1035–1042. https://doi.org/10.1016/S0016-5085(99)70006-5.

Doss, B.L., et al., 2019. Quantitative mechanical analysis of indentations on layered, soft elastic materials. Soft Matter 15 (8), 1776–1784. https://doi.org/10.1039/C8SM02121J.

Fan, X.P., et al., 2013. Sonographic evaluation of proximal gastric accommodation in patients with functional dyspepsia. World J. Gastroenterol. 19 (29), 4774–4780. https://doi.org/10.3748/wjg.v19.i29.4774.

Febo-Rodriguez, L., et al., 2021. Gastric Accommodation: Physiology, Diagnostic Modalities, Clinical Relevance, and Therapies. Neurogastroenterology and Motility, pp. 1–15. https://doi.org/10.1111/nmo.14213. May.

Gregersen, H., Christensen, J., 2000. Gastrointestinal tone. Neuro Gastroenterol. Motil. 12 (6), 501–508. https://doi.org/10.1046/j.1365-2982.2000.00233.x.

Janssen, P., et al., 2011. Intragastric pressure during food intake: a physiological and minimally invasive method to assess gastric accommodation. Neuro Gastroenterol. Motil. 23 (4) https://doi.org/10.1111/j.1365-2982.2011.01676.x.

Kim, D.Y., Camilleri, M., 2002. Noninvasive measurement of gastric accommodation by SPECT. Kor. J. Intern. Med. 17 (1), 1–6. https://doi.org/10.3904/kjim.2002.17.1.1.

Kindt, S., Tack, J., 2006. Impaired gastric accommodation and its role in dyspepsia. Gut 55 (12), 1685–1691. https://doi.org/10.1136/gut.2005.085365.

Kwiatek, M.A., et al., 2009. Effect of meal volume and calorie load on postprandial gastric function and emptying: studies under physiological conditions by combined fiber-optic pressure measurement and MRI. Am. J. Physiol. Gastrointest. Liver Physiol. 297 (5), 894–901. https://doi.org/10.1152/ajpgi.00117.2009.

Kay, L., Jørgensen, T., 1994. Epidemiology of upper dyspepsia in a random population. Prevalence, incidence, natural history, and risk factors - PubMed. Scand. J. Gastroenterol. 29 (1), 2–6. Available at: https://pubmed.ncbi.nlm.nih.gov/8128172/. (Accessed 13 September 2021). Accessed:

Mott, P.H., Dorgan, J.R., Roland, C.M., 2008. The bulk modulus and Poisson's ratio of "incompressible" materials. J. Sound Vib. 312 (4–5), 572–575. https://doi.org/10.1016/J.JSV.2008.01.026.

Olafsdottir, E., et al., 2000. Impaired accommodation of the proximal stomach in children with recurrent abdominal pain. J. Pediatr. Gastroenterol. Nutr. 30 (2), 157–163. https://doi.org/10.1097/00005176-200002000-00012.

Piessevaux, H., et al., 2001. Perception of changes in wall tension of the proximal stomach in humans. Gut 49 (2), 203–208. https://doi.org/10.1136/gut.49.2.203.

Van Ramshorst, G.H., et al., 2011. Noninvasive assessment of intra-abdominal pressure by measurement of abdominal wall tension. J. Surg. Res. 171 (1), 240–244. https://doi.org/10.1016/j.jss.2010.02.007.

Sneddon, I.N., 1965. The relation between load and penetration in the axisymmetric boussinesq problem for a punch of arbitrary profile. Int. J. Eng. Sci. 3 (1), 47–57. https://doi.org/10.1016/0020-7225(65)90019-4.

Staunton, J.R., et al., 2016. Correlating confocal microscopy and atomic force indentation reveals metastatic cancer cells stiffen during invasion into collagen i matrices. Sci. Rep. 6 (January), 1–15. https://doi.org/10.1038/srep19686.

Steinsvik, E.K., et al., 2021. Ultrasound imaging for assessing functions of the GI tract. Physiol. Meas. 42 (2) https://doi.org/10.1088/1361-6579/ABDAD7.

Sun, W., Paulose, J., 2021. Indentation responses of pressurized ellipsoidal and cylindrical elastic shells: insights from shallow-shell theory. Phys. Rev. 104 (2), 1–17. https://doi.org/10.1103/PhysRevE.104.025004.

Tang, H., et al., 2021. A new device for measuring abdominal wall tension and its value in screening abdominal infection. Medical devices (Auckland, N.Z.) 14, 119–131. https://doi.org/10.2147/MDER.S291407.

Tayebi, S., et al., 2021. A concise overview of non-invasive intra-abdominal pressure measurement techniques: from bench to bedside. J. Clin. Monit. Comput. 35 (1), 51–70. https://doi.org/10.1007/s10877-020-00561-4.

Tefera, S., et al., 2001. Gastric accommodation studied by ultrasonography in patients with reflux esophagitis. Dig. Dis. Sci. 46 (3), 618–625. https://doi.org/10.1023/A:1005619803917.

Toniolo, I., et al., 2022. Coupled experimental and computational approach to stomach biomechanics: towards a validated characterization of gastric tissues mechanical properties. J. Mech. Behav. Biomed. Mater. 125, 104914 https://doi.org/10.1016/J.JMBBM.2021.104914.

Undeland, K.A., et al., 1998. Gastric meal accommodation studied by ultrasound in diabetes: relation to vagal tone. Scand. J. Gastroenterol. 33 (3), 236–241. https://doi.org/10.1080/00365529850170784.

Vella, D., et al., 2012. The indentation of pressurized elastic shells: from polymeric capsules to yeast cells. J. R. Soc. Interface 9 (68), 448–455. https://doi.org/10.1098/rsif.2011.0352.

Wolf, A.T., Descamps, P., 2002. 'Determination of Poisson's Ratio of Silicone Sealants from Ultrasonic and Tensile Measurements'. ASTM Special Technical Publication, pp. 132–142. https://doi.org/10.1520/STP10932S, 1422.

Zhao, J., et al., 2008. Stomach stress and strain depend on location, direction and the layered structure. J. Biomech. 41 (16), 3441–3447. https://doi.org/10.1016/J.JBIOMECH.2008.09.008.

De Zwart, I.M., et al., 2007. Gastric accommodation and motility are influenced by the barostat device: assessment with magnetic resonance imaging. Am. J. Physiol. Gastrointest. Liver Physiol. 292 (1), 1–24. https://doi.org/10.1152/ajpgi.00151.2006.